ELSEVIER

Surface Science 499 (2002) 109–123

SURFACE SCIENCE

www.elsevier.com/locate/susc

Functionalizing the GaN(0 0 0 1)-(1 × 1) surface I. The chemisorption of aniline

V.M. Bermudez *

Naval Research Laboratory, Code 6862, 4555 Overlook Avenue, S.W., 20375-5347 Washington, DC, USA

Received 19 September 2001; accepted for publication 26 November 2001

Abstract

Chemisorption of aniline ($C_6H_5NH_2$) on the GaN(0 0 0 1)-(1 × 1) Ga-polar surface has been studied using mainly X-ray-excited Auger electron, electron energy loss and ultraviolet photoemission spectroscopies (XAES, ELS and UPS, respectively). The XAES data show adsorption near room temperature with a total sticking probability of ~0.05 and a saturation coverage of ~0.28 phenyl rings per surface lattice site. The ELS data show removal of the characteristic surface-state band centered at ~3.4 eV and the appearance of a $\pi \rightarrow \pi^*$ loss at 6.5 eV due to C=C bonds. In contrast, benzene (C_6H_6) does not chemisorb under these conditions. The UPS data, which have been analyzed with the aid of density functional theory molecular orbital calculations, indicate that adsorption occurs with a phenyl–NH group forming a Ga–N–Ga bridge. Adsorption causes a decrease in electron affinity ($\delta\chi \approx -0.55$ eV) due to a surface dipole layer, and measurement of $\delta\chi$ and of changes in band bending have been used to construct a partial energy level diagram for the aniline-covered surface.

Keywords: Gallium nitride; Aromatics; Chemisorption; Photoelectron spectroscopy; Auger electron spectroscopy; Electron energy loss spectroscopy (EELS)

1. Introduction

The recent acceleration of interest in "molecular electronics" has led to numerous studies of the attachment of organic ligands to the surfaces of semiconductors, primarily Si(1 0 0) and Si(1 1 1) [1–3] and also II–VI and III–V materials [4]. Potential applications for such "functionalized" semiconductor surfaces include chemical- and biosensors, nanoscale electronic components (e.g., switches and transistors), new devices for the emission and detection of light and novel alternatives to lithographic patterning for nanofabrication.

Extending this work to wide-bandgap materials such as SiC and GaN offers advantages over the use of Si as a substrate. In optoelectronic devices, the wide bandgap of 6H–SiC (3.0 eV) or GaN (3.4 eV) permits optical access to the organic layer through the substrate as well as through space, permitting more flexibility in device design. In applications dependent on charge transport across the interface, the wide bandgap also allows more

* Fax: +1-202-404-4071.

E-mail address: bermudez@estd.nrl.navy.mil (V.M. Bermudez).

0039-6028/02/$ - see front matter
PII: S0039-6028(01)01916-1

latitude in aligning the highest occupied and lowest unoccupied molecular orbitals (HOMO and LUMO, respectively) of the organic adsorbate with the substrate band edges. This opens the possibility, for example, of molecular control of the semiconductor electronic properties [4–6].

Functionalizing GaN surfaces requires new chemical strategies. Recently [7] NH_3 has been shown to chemisorb on the clean (0 0 0 1)-(1 × 1) Ga-polar surface of wurtzite GaN via a stable asymmetric Ga–(NH_2)–Ga bridge. This suggests that amine chemistry may be a viable approach to building organic structures on such surfaces. To our knowledge there has been no previous work on functionalizing III-nitride surfaces other than studies of the adsorption of organic species on AlN [8] or GaN [9] nanoparticles.

In this work, we focus on the electronic structure and properties of the GaN(0 0 0 1)-(1 × 1) surface functionalized by adsorption of aniline, the molecular structure of which is shown in Fig. 1. This amine was selected for initial study because it has been investigated as an adsorbate on Si(1 0 0)-(2 × 1) [10–14] and (1 1 1)-(7 × 7) [15] surfaces and because GaN surfaces functionalized with aniline

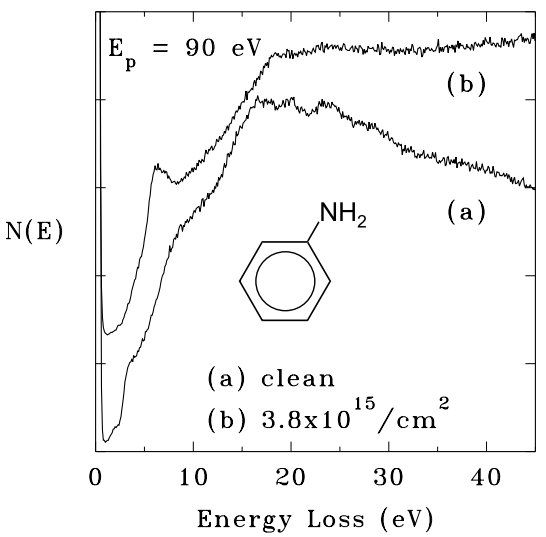

Fig. 1. ELS data (a) before and (b) after dosing with aniline. In (b) the dose is given as the number of aniline molecules incident per cm^2. The relative intensity is quantitative, and the spectra have been displaced vertically for clarity. The inset shows the molecular structure of aniline.

or substituted anilines might be suitable for subsequent chemical or photochemical reaction, providing a means for in situ synthesis of larger and more complex surface species.

2. Experimental details

All experiments were performed in a conventional ultra-high vacuum (UHV) chamber with a base pressure of $\sim 5 \times 10^{-11}$ Torr. The n-type wurtzite GaN sample, grown on sapphire by metal–organic chemical vapor deposition, was cut from the same wafer as that used in a previous study of H_2O adsorption and is described elsewhere [16]. The surface was cleaned by nitrogen-ion bombardment (10 min, 1 keV, ~10 μA/cm^2) and annealing (5 min, ~900 °C) [17,18]. The clean surface exhibited no impurities in Auger electron spectroscopy (AES), other than sometimes oxygen at the limit of detection. Based on previous studies of O_2 chemisorption [17], this limit is ~0.03 monolayers (MLs), where 1 ML is defined as one adsorbate species per surface lattice site. Low-energy electron diffraction (LEED) showed the (1 × 1) pattern typical for GaN(0 0 0 1) surfaces prepared in this manner. The LEED pattern for this particular sample showed a somewhat higher background than usual but little or none of the faceting normally found for such surfaces [18–20]. The lattice polarity [21] was found [16] to be such that the surface under study was the (0 0 0 1) Ga-polar face.

Ultraviolet photoemission spectroscopy (UPS) and electron energy loss spectroscopy (ELS) were performed using a double-pass cylindrical-mirror analyzer (CMA) in the constant-resolution (''retard'') mode with pulse-count detection. For UPS, the 40.8 eV HeII line from a DC discharge in He was used. The Fermi level position was measured using UPS data for a clean Au foil. The resolution, determined by the CMA pass energy of 50 eV, was about 0.80 eV as measured by the Gaussian broadening of the Au Fermi edge. The photoelectron work function was obtained by measuring the slow-secondary photoemission threshold with a −5.8 V bias applied to the sample, to shift the edge well above the CMA cutoff, and with the

nominal CMA resolution increased to ~30 meV. For ELS, a primary beam of $E_p \approx 90$ eV and $i_p \approx 0.3$ μA/cm^2 from the coaxial electron gun of the CMA was incident normal to the sample surface. The resolution, defined by the full-width at half-maximum (FWHM) of the elastic peak, was 0.5 eV.

X-ray-excited AES (XAES) C KLL and N KLL data were obtained in pulse-count "retard" mode using the 1253.6 eV Mg $K\alpha_{1,2}$ line with a resolution of ~3.2 eV, determined by the CMA pass energy of 200 eV. The C 1s X-ray photoemission spectrum (XPS) was obtained at a resolution of ~1.6 eV (100 eV CMA pass energy) using the 1486.6 eV Al $K\alpha_{1,2}$ line. The binding energy (BE) was referenced to the Au $4d_{5/2}$ and $4f_{7/2}$ lines at 335.22 and 83.98 eV, respectively, below E_F [22]. Because of the likelihood of electron-beam damage of adsorbed molecules, electron-excited AES (EAES) was used only to check the surface elemental composition. For EAES, a primary beam of $E_p = 3$ keV, $i_p \approx 4.5$ μA from the coaxial electron gun was incident normal to the surface, and the CMA was used in the "non-retard" mode with a 2 eV modulation amplitude.

Aniline, obtained commercially, was dried by distillation under vacuum onto Na metal and degassed by repeated freeze–pump–thaw cycles, with freezing at dry-ice temperature. At least one such cycle was performed prior to each exposure to remove H_2 released during contact between aniline and Na. The aniline reservoir was kept in the dark to avoid photochemical reactions. Benzene, also obtained commercially, was used without further purification other than degassing. Analyses of the vapors exiting the doser (see below) were done using a quadrupole mass spectrometer on the UHV chamber, at a reagent pressure of $\sim 5 \times 10^{-7}$ Torr with continuous turbopumping. These showed no significant impurities when referenced to standard cracking patterns. [1] In particular, there was no difference between the mass spectra of the "as-received" and dried aniline other than the presence of a significant amount of H_2O in the former.

Gas exposures were done using a pinhole doser [23]. During and after dosing, the hot-filament ionization gauge was switched off and the chamber pressure measured with a cold-cathode ionization gauge to avoid excitation of molecular species in the background. During dosing, the ion pump was also switched off and the chamber pumped with a turbopump to avoid regurgitation when ion-pumping reactive species. During and after dosing the chamber viewports were covered and the sample kept in the dark, as much as possible, to avoid potential photochemical effects. However, no effect of intentional exposure to visible light was noted in UPS or work-function data (see below) for the aniline-saturated surface. All dosing and data scans were done with the sample at nominal room temperature (< 50 °C).

3. Results and discussion

3.1. ELS and XAES

Figs. 1 and 2 show ELS data for clean and aniline-dosed surfaces. In common with other adsorbates (O_2 [17] and atomic H [18,24,25]) aniline removes the surface-state loss feature characteristic of the clean surface. This consists of a band centered at about 3.4 eV with a tail extending into the gap. A very weak adsorbate-sensitive feature, possibly due to surface defects, also appears at ~2 eV for the clean surface. The major feature after exposure, at 6.5 eV, corresponds to $\pi \rightarrow \pi^*$ excitation of the phenyl ring [26], and the presence of this feature proves the existence of π-bonded C on the surface. The near coincidence in energy with the most intense free-molecule loss peak (6.49 eV, [26]) suggests that the ring does not interact strongly with the surface via the π-orbitals.

The dose dependence of the ELS data was studied as a measure of the rate of adsorption since the spectra could be acquired relatively quickly. After each dose, the aniline was evacuated and the 0–16 eV range scanned. The incident beam spot size was ~1 mm, allowing a different area of the surface to be sampled after each dose to avoid any

[1] The aniline and benzene cracking patterns, from the NIST/EPA/NIH Mass Spectral Library, were obtained at http://webbook.nist.gov/chemistry.

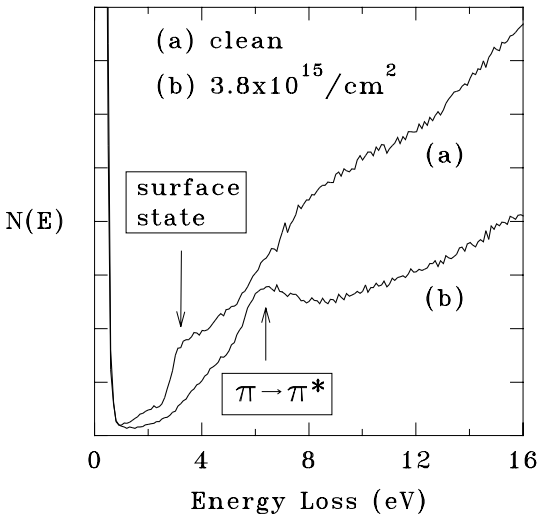

Fig. 2. Similar to Fig. 1 but showing the low-energy losses in detail. The surface-state loss on the clean surface and the $\pi \rightarrow \pi^*$ transition on the dosed surface are labelled. Relative intensities are not quantitative.

cumulative beam-damage effects. (No such effects, however, were observed in repeated scans of the same area.) Beyond a dose of $\sim 6 \times 10^{15}$ aniline/cm^2 there were no further significant changes in the spectrum, indicating that saturation had occurred. [2] After saturation and several hours of data collection, EAES indicated a trace of O which might be due to H_2O in the UHV background or as a residual impurity in the aniline. It has previously been found [16] that H_2O is highly reactive with the clean GaN(0 0 0 1)-(1 × 1) surface. The LEED pattern at saturation was a very weak (1 × 1) with a high background. It is likely, however, that the LEED primary beam (about 50 eV and 50 μA/cm^2) would damage any adsorbed molecules.

Fig. 3 shows C KLL and N KLL XAES data at saturation after background removal as described in Appendix A. The N KLL, in comparison to that of the bare surface (not shown), exhibited no additional structure that might be due to N bonded

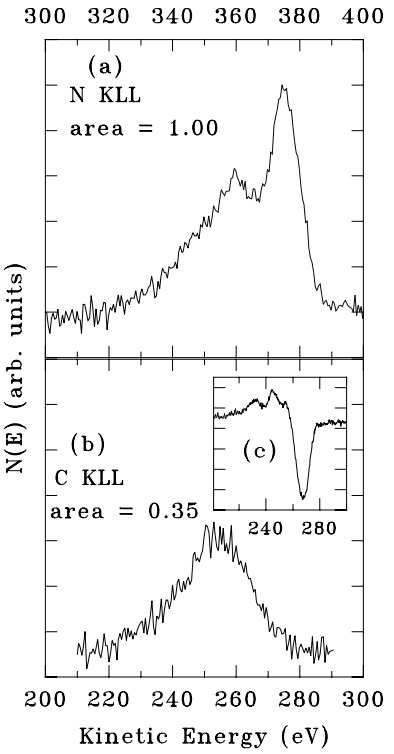

Fig. 3. XAES data for the (a) N KLL and (b) C KLL transitions on the aniline-saturated surface after processing as described in Appendix A. Relative intensities are not quantitative, but the relative C KLL/N KLL integrated area is given. The inset (c) shows the lineshape observed in first-derivative EAES data.

to a phenyl ring. For five different runs, the coverage of C (viz. phenyl rings) was estimated from the relative integrated intensities (see Appendix A). The result is $\Theta_{ph} = 0.28 \pm 0.05$ ML, where $\Theta_{ph} = 1$ is defined as 1 phenyl ring per surface lattice site. (The uncertainty reflects scatter in the data and does not include the effects of any systematic errors in the model given in Appendix A.) The results give a total sticking probability, defined here as (saturation coverage)/(saturation dose), of ~0.05 which indicates that aniline is very reactive with this surface.

Similar ELS and AES experiments were done with benzene. A dose of $\sim 3.5 \times 10^{16}$ benzene/cm^2, i.e., about six times the aniline dose needed for saturation, had little or no effect on the GaN surface-state loss and produced no significant

[2] For reference, the GaN(0 0 0 1) surface plane consists of 1.135×10^{15} lattice sites per cm^2, based on a basal-plane lattice constant of 3.1892 Å.

$\pi \rightarrow \pi^*$ peak. Little or no C KLL intensity was detected in either XAES or EAES. Hence benzene is much less reactive than aniline under the same conditions. This argues against an adsorption process involving *only* C–H bond breaking or *only* the ring π-orbitals. (The latter is seen for benzene on transition metals, e.g. [27] and works cited.) However, it cannot be inferred from this observation alone that aniline adsorption occurs via the $–NH_2$ since the substituent effect of the $–NH_2$, well known in organic chemistry, alters the charge distribution in the ring π-orbitals.

3.2. UPS

Fig. 4 shows UPS data for the clean surface before and after a saturation exposure. In Fig. 4a the peak at −20.5 eV is the Ga 3d, the weak broad peak near −17 eV is the N 2s and the peak at about −13 eV is a "ghost" of the Ga 3d excited by the $h\nu = 48.4$ eV satellite of the main HeII line. Other, weaker satellites contribute additional "ghost" intensity near −9 eV. Note the reduction in Ga 3d intensity, relative to the valence band, after aniline adsorption. This shows that the substrate emission is significantly attenuated by the adsorbate layer and, therefore, that a large fraction of the valence intensity in Figs. 4b and c is due to the adsorbate.

The UPS of the adsorbate itself, Fig. 5a, was obtained from the difference, $\Delta N(E)$, between the data in Figs. 4a and b by scaling and shifting the clean-surface spectrum so as to minimize the residual Ga 3d intensity after subtraction. The effect of molecular chemisorption on the Ga 3d of GaN(0 0 0 1)-(1 × 1) is generally quite small [16, 17], so good cancellation in $\Delta N(E)$ is expected. The result shows strong emission at the high-BE end, due to excitation by the more intense HeI line ($h\nu = 21.2$ eV), but no Ga 3d feature (cf. Fig. 4). Data obtained at higher resolution (0.4 eV with a 25 eV CMA pass energy) showed no additional structure in $\Delta N(E)$.

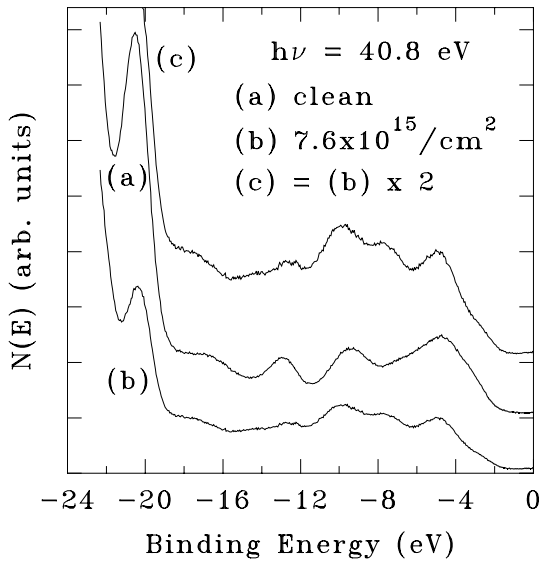

Fig. 4. HeII UPS data (a) before and (b) after dosing with aniline. Binding energies are referenced to the Fermi level, and the spectra have been displaced vertically for clarity. The relative intensity is not quantitative. (c) shows the same spectrum as (b), multiplied by a factor of 2 for easier comparison with (a).

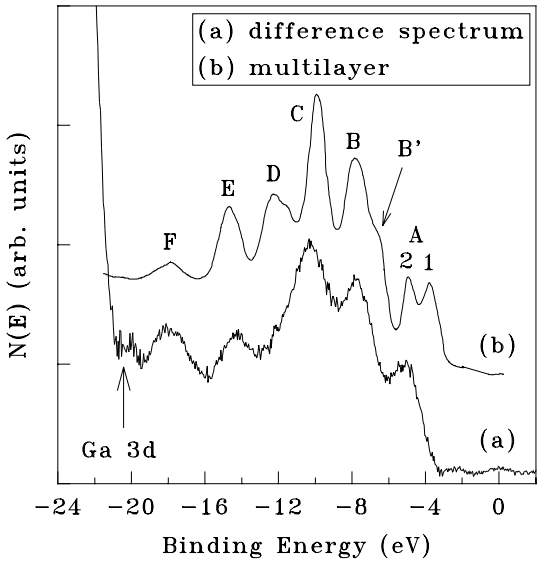

Fig. 5. (a) Difference spectrum (dosed minus clean) obtained from the data in Fig. 4. The arrow shows where the Ga 3d peak was prior to subtraction. The clean-surface spectrum was scaled and shifted so as to minimize the Ga 3d intensity in the difference. The intense emission at the low-BE end is due to HeI excitation. (b) UPS data ($h\nu = 34$ eV) for a condensed multilayer of aniline [30, with permission]. The labels "A", "B", etc. are those in the original reference. The two A peaks are further labelled "1" and "2", and the shoulder of peak B is labelled "B′". The relative intensity of the two spectra is not quantitative. The two spectra have been aligned at the deep-valence level "F", and binding energies are referenced to the Fermi level.

For adsorbates such as NH_3 [7], O_2 [17,28] or atomic H [18] on GaN(0 0 0 1)-(1 × 1), UPS $\Delta N(E)$ spectra show a pronounced "negative" (i.e., downward-pointing) peak at about −2.8 eV due to removal of surface states near the valence band maximum (VBM) on the clean surface [29]. There is little if any indication of such a feature in Fig. 5a because of the strong attenuation of the substrate emission by the aniline adlayer. It is also possible that the absence of this negative feature is due to an adsorbate peak which exactly matches the position and intensity of the surface-state emission on the clean surface, thereby yielding a featureless $\Delta N(E)$ in this region. This was investigated by repeating the subtraction process for different clean-surface scale factors. Although a negative peak near the VBM could be produced with small adjustments in the scale factor, it was not possible to obtain even a weak positive (i.e., adsorbate-related) peak in this part of $\Delta N(E)$ without a pronounced miscancellation of the Ga 3d.

Fig. 5b shows UPS data ($h\nu = 34$ eV) for a multilayer of aniline condensed on Pd(1 1 0) [30]. This spectrum is in good agreement with, although less resolved than, gas-phase HeII data [31]. The rough similarity between the adsorbed and multilayer spectra suggests adsorption with the phenyl ring intact. This is supported by comparison with data (not shown), obtained at $h\nu = 50$ eV, for a benzene multilayer condensed on Si(1 0 0)-(2 × 1) [32]. The major peaks in the benzene spectrum agree with those of adsorbed aniline in number and relative position, although, as noted above, molecular benzene itself does not adsorb readily on this GaN surface.

In order to compensate for differences in screening and relaxation of the photoionized molecule [33] between the two phases, the multilayer spectrum (Fig. 5b) was shifted to bring peak "F" into alignment with that of the adsorbate (Fig. 5a). The required shift (0.7 eV to higher BE) represents the result of differences in sample work function and in relaxation effects for aniline adsorbed on GaN(0 0 0 1) and condensed on Pd(1 1 0). Deep-valence orbitals, such as those contributing to peak "F", are expected to be essentially unaffected by adsorption chemistry. After this alignment, peak "C" shows a further small BE difference indicating an additional chemical shift due to adsorption. The shoulder B′ in the multilayer spectrum is assigned [31,34] to the N non-bonding lone-pair (NBLP) orbital, which is confirmed by MO calculations discussed below. It is not certain whether this feature is shifted, broadened or altogether absent in the adsorbate spectrum. Hence, adsorption with N remaining in threefold coordination, unlike the case for NH_3 on this surface [7], cannot be ruled out at this point. One also cannot yet exclude adsorption via formation of a donor–acceptor adduct involving charge donation from the nitrogen NBLP orbital to a Ga dangling orbital.

The most obvious difference between the two spectra in Fig. 5 is the absence of peaks for the adsorbed layer corresponding to A1 (the HOMO of the condensed molecule) and to D. MO calculations (see below) show that both A1 and D involve large contributions from the $-NH_2$ group, and their absence indicates that adsorption involves this part of the molecule. It is unlikely that polymerization of the adsorbed aniline plays a significant role since UPS data for various forms of polyaniline [35] show only relatively broad structures.

There is presently no basis for determining the fate of any H atoms released in chemisorption since the UPS $\Delta N(E)$ is dominated by excitations of the molecular species, with no evidence of features that can clearly be assigned to adsorbed H alone. Changes in the GaN surface electronic structure (e.g., removal of surface states) caused by molecular adsorption would also affect $\Delta N(E)$. However, here again the spectrum appears to consist mainly of molecular features. The data will be discussed in more detail in Section 3.6, in the context of different chemisorption models.

3.3. XPS

The C 1s XPS, Fig. 6, gave no indication of structure and could be least-squares fitted with a single Gaussian at 285.7 ± 0.1 eV below E_F. After subtracting the instrumental broadening in quadrature, the FWHM was ~2.8 eV. The presence of a single C 1s coincides with results for aniline forming an Si–N–Si bridge on the Si(1 0 0)-

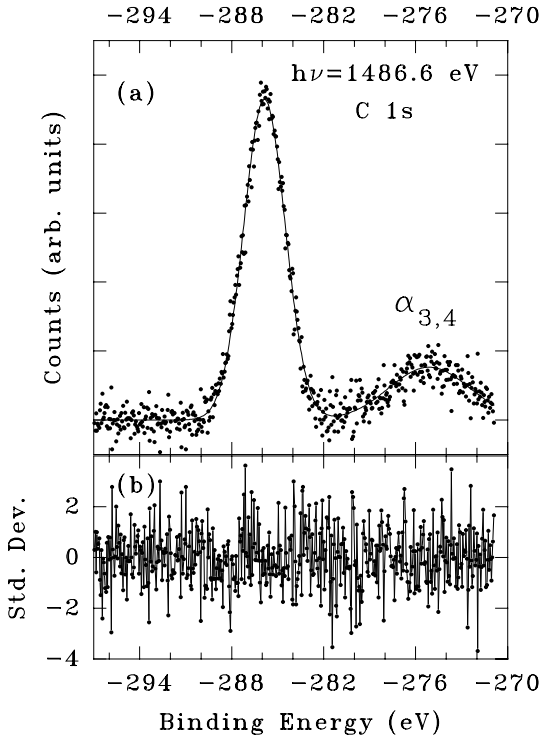

Fig. 6. (a) C 1s XPS (Al $K\alpha_{1,2}$ excitation) for the aniline-saturated surface. The feature labelled "$\alpha_{3,4}$" is the C 1s excited by satellites in the source spectrum. The points show data (average of three scans), and the line gives a least-squares fit of a sum of Gaussians and a polynomial background. (b) Spectrum of statistically weighted residuals [(fit-data)/data$^{1/2}$] which gives a reduced χ^2 of 1.30.

(2×1) surface [13] and for molecular aniline condensed on Ni(1 0 0) at 100 K [36]. This suggests that the phenyl ring is at most only weakly perturbed by adsorption, a view which will be supported by the analysis of the C 1s BE presented below.

For aniline on Si(1 0 0)-(2×1) [14] the C 1s XPS can be resolved into components with FWHM of ~0.8 eV, substantially less than on GaN. The greater FWHM in the case of GaN results in part from the vibrational broadening of XPS lines typical for partially ionic materials as well as from possible band-bending inhomogeneity (e.g., [37]). However, the bulk GaN Mg $K\alpha_{1,2}$-excited N 1s line (not shown) has an FWHM of only ~1.7 eV after correction for instrumental broadening. This suggests that a large part of the 2.8 eV C 1s FWHM for aniline on GaN(0 0 0 1) is due to the presence of unresolved, closely spaced components.

Since available C 1s XPS data for condensed aniline multilayers [36,38] do not give the position of the vacuum level, it is necessary to estimate the chemical shift in the C 1s BE by comparing the data in Fig. 6 with gas-phase results [39]. These show C 1s BEs, relative to vacuum, of 291.2 eV for the C bonded to $–NH_2$ and in the range of 289.7–290.2 eV for the others. To avoid difficulties in BE referencing, the C 1s BE shift is estimated here using the difference, Δ(BE), between the C 1s and a deep-valence feature ("F" in Fig. 5a) which is affected only by relaxation, not chemisorption, as discussed above. The change in Δ(BE) between the gas and adsorbed phases is then taken as the C 1s BE shift due to surface chemical effects. Using gas-phase data in [31,39] and adsorbate data in Figs. 5a and 6, and taking 290.2 eV as the average C 1s gas-phase BE, yields a chemical shift of about 0. This, together with observation of only a single C 1s, suggests that the phenyl ring is not strongly affected by chemisorption.

The N 1s XPS data for adsorbed aniline (BE $\approx$ 398 eV [13]) could not be obtained with either Mg or Al $K\alpha_{1,2}$ excitation because of interference from overlapping Ga LMM XAES structure and because of the high background from bulk N 1s emission.

3.4. Work function, band bending and electron affinity

The effects of aniline adsorption on band bending and electron affinity were studied in order to establish an energy level diagram for the surface after chemisorption.

The UPS data were used to obtain the change in electron affinity ($\delta\chi = \delta\phi - \delta\phi_B$) from the changes in work function ($\delta\phi$) and band bending ($\delta\phi_B$), where $\delta\phi_B > 0$ means an increase in upward band bending for n-type GaN. Fig. 7 shows the relevant data, namely, the positions of the Ga 3d core level (upper panel) and the slow-secondary threshold (lower panel) for clean and for aniline-saturated surfaces. The quantities obtained in Fig. 7 are

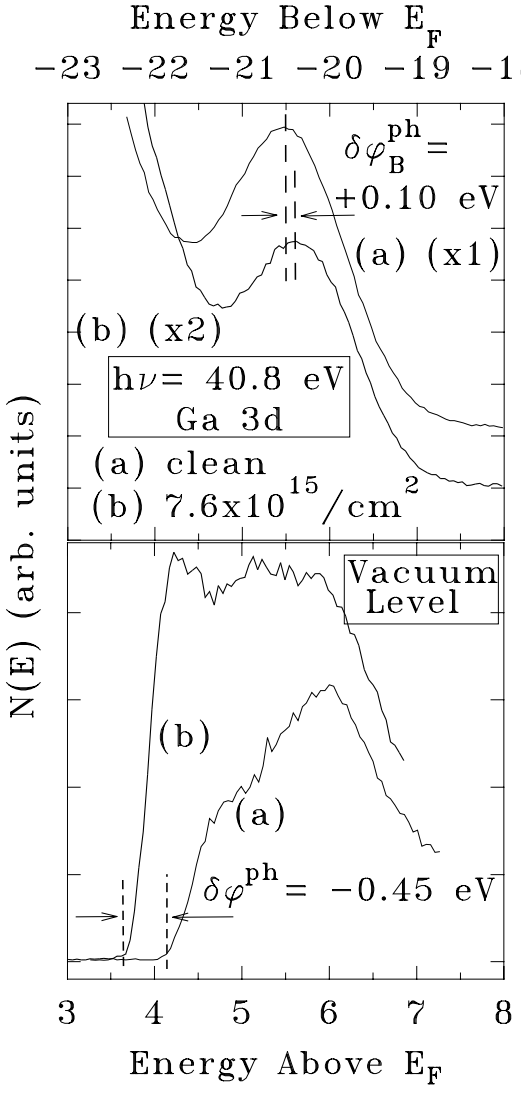

Fig. 7. UPS data showing the change in band bending (upper panel) and the change in work function (lower panel) induced by a saturation dose of aniline. Note the different energy scales. Relative intensities are not quantitative. The upper panel shows the Ga 3d spectra from Fig. 4 with (b) multiplied by a factor of 2, relative to (a), for clarity. The dashed lines show the respective peak maxima, indicating $\delta\phi_B^{ph} = +0.10$ eV, where "ph" denotes "photoelectron value" (see text). In the lower panel the dashed lines show the respective energies of the sample vacuum level, estimated by extrapolating the edge of the slow-secondary emission to zero, which give $\delta\phi^{ph} = -0.45$ eV.

labelled "$\delta\phi_B^{ph}$" and "$\delta\phi^{ph}$", indicating that they are photoelectron values (see below). Structure in the near-threshold emission is related to empty states at or above the vacuum level; the shape of the spectrum is affected by the work function cutoff, though. The spectrum clearly changes with aniline adsorption, but further analysis is beyond the scope of the present work.

With the expression given above, results like those in Fig. 7 yield $\delta\chi = -0.55 \pm 0.13$ eV (average of four runs). Using the adsorbate coverage at saturation (Section 3.1), an estimate of the surface-normal dipole moment $\mu_\perp$ (in Debyes, D, where 1 D $= 10^{-18}$ esu cm) can be obtained from the expression $\delta\chi(\text{eV}) = 3 \times 10^{-16}(4\pi N\mu_\perp)$ for a layer of N non-interacting dipoles per cm^2. The result is $\mu_\perp = -0.45$ D, where the negative sign means that the positive end of the dipole lies outward from the surface. The effect of depolarization by surrounding dipoles can be estimated using [40] $\mu_\perp = \mu_\perp(0)/(1 + 9\alpha N^{3/2})$, where $\mu_\perp(0)$ is the moment of an isolated adsorbed dipole and α is the adsorbate polarizability. With $\alpha = 11.5 \times 10^{-24}$ cm^3 for free aniline [3] [41], $\mu_\perp(0) \approx -0.72$ D is found, which amounts to a large correction. This result is somewhat smaller in magnitude than the in-plane and out-of-plane components of the gas-phase aniline dipole moment [42], 1.07 and 1.09 D respectively. Quantitative interpretation of $\mu_\perp(0)$ in terms of a structural model (see below) is difficult since it represents the combined effects of the molecular dipole moment, modified by adsorption, and charge transfer between the surface and the adsorbate.

The UPS data were examined for the effects of surface photovoltage (SPV) caused by electron-hole (e–h) pairs created by the UV excitation and by inelastic scattering of photoelectrons and secondaries. An SPV effect occurs in semiconductors when e–h pairs separate in the space–charge field, leading to a decrease in band bending vs the true ("in-the-dark") value. For n-type material, the decreased band bending is equivalent to a decreased photoelectron work function, i.e, $\phi^{ph} \leqslant \phi$ where ϕ is the true work function. Such effects

[3] $\alpha = \frac{1}{3}(\alpha_{xx} + \alpha_{yy} + \alpha_{zz})$ is the average of the diagonal tensor components.

have been studied extensively (e.g., [43] and works cited) and are observed for GaN(0 0 0 1)-(1 × 1) surfaces after chemisorption of H_2O but to a much lesser extent when clean [16]. Note that SPV is a purely electrostatic effect, shifting ϕ^{ph} and ϕ_B^{ph} equally, so that $\delta\chi$ is unaffected. Stated differently, any change in band bending causes identical shifts relative to E_F in the vacuum level, band edges and core levels (assuming that the photoelectron escape depth in each case is much less than the thickness of the space–charge layer).

Following [43], the temperature dependence of the Ga 3d BE was measured. Since the e–h recombination rate increases with temperature, the SPV effect (if present) will decrease. For n-type material this results in a reversible, temperature-dependent rigid shift of core levels to lower BE with increasing temperature as the SPV effect on ϕ_B^{ph} is reduced. The results for the aniline-saturated surface (not shown) indicate a shift of about −0.13 eV in Ga 3d BE, over the range of 38–130 °C. Similar experiments on clean surfaces show an SPV shift of < 0.1 eV in magnitude (i.e., at or near the detection limit). In principle, the true $\delta\phi$ and $\delta\phi_B$ could be obtained by increasing the sample temperature until $\delta\phi^{ph}$ and $\delta\phi_B^{ph}$ become constant, i.e., until the SPV has been eliminated [43]. However, this is impractical here because of possible thermally induced changes in the adsorbate layer. If a true $\delta\phi$ can be measured, a true $\delta\phi_B$ can be estimated using the previously obtained $\delta\chi \approx -0.55$ eV which is independent of SPV as noted above.

A measurement of $\delta\phi$ in the absence of optical or electronic excitation was attempted using a piezoelectrically driven Kelvin probe [44] to record the change, due to adsorption of aniline, in the contact potential difference (CPD) between the sample and an Au-plated vibrating probe. The *apparent* $\delta\phi$ measured this way was more positive than $\delta\phi^{ph} = -0.45$ eV (Fig. 7), consistent with the absence of an SPV effect. However, a complicating factor is the possible adsorption of aniline on the (dirty) Au surface as well as on the GaN, since $\delta\phi_{Au} < \delta\phi_{GaN} < 0$ would yield a positive change in CPD. To our knowledge, $\delta\phi_{Au}$ has not been studied for aniline adsorption; however, data for aniline on clean Pd(1 1 0) [30] and Pt(1 0 0) and (1 1 1) [45] surfaces show $\delta\phi_{Pd} = -1.55$ eV and $\delta\phi_{Pt} \approx -1.8$ eV at saturation.

Since even a small coverage of aniline on the Au Kelvin probe could have a significant effect on the CPD, the temperature dependence of the Ga 3d BE given above is used to estimate the SPV effect on band bending. The result, $\delta\phi_B \geqslant \delta\phi_B^{ph} + 0.13$ eV $= +0.23$ eV, constitutes a lower limit on the true change in band bending due to aniline adsorption.

3.5. Energy level alignment

Fig. 8 shows a partial energy level diagram deduced from experimental quantities given above and elsewhere. The bulk bandgap of $E_g = 3.4$ eV separates the VBM from the conduction band minimum (CBM). The position of the Fermi level (E_F) in the bulk, ~0.07 eV below the CBM at room temperature, was computed [46] for a non-degenerate CBM using the donor density of 1.6×10^{17}/cm^3 and an isotropic electron effective mass, $m^* = 0.236m_e$ [47]. The position of E_F at the surface (~0.9 eV below the CBM) was obtained from

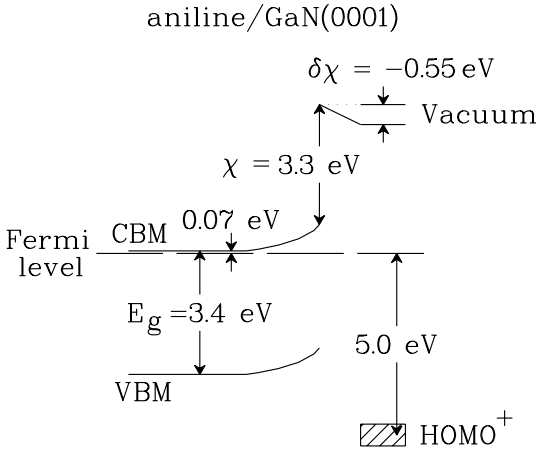

Fig. 8. Partial energy level diagram (only one adsorbate level included) for a saturation coverage of aniline adsorbed on GaN(0 0 0 1)-(1 × 1). The physical dimensions (e.g., the thicknesses of the space–charge and dipole layers) are not to scale, but the energy separations of the various levels are scaled quantitatively. The label "HOMO$^+$" emphasizes that the level is that of the photoionized adsorbate. The width of the HOMO$^+$, indicated by the box, is estimated from the width in UPS after correcting for instrumental broadening.

the measured E_F–Ga 3d separation (Fig. 7) after subtracting the VBM–Ga 3d energy difference (17.76 eV, [48]) which is a material constant. This E_F position has been corrected for the estimated SPV effect during UPS, as described above. The clean-surface electron affinity, $\chi = 3.3$ eV, was measured previously [17,28], and the change $\delta\chi$ associated with the surface dipole layer was given in Section 3.3.

The position of the HOMO of the photoionized adsorbate ("$HOMO^+$" in Fig. 8) relative to E_F was observed in Fig. 5a and the width (~0.6 eV) estimated from the FWHM after subtracting the instrumental broadening in quadrature. The charge transport gap, the quantity of interest in charge transport phenomena, is given [49,50] by the separation between $HOMO^+$ and $LUMO^-$, the level formed by placing an electron into the LUMO of the neutral adsorbate. The $LUMO^-$ position relative to E_F can best be determined by inverse photoemission spectroscopy [49,50]. For a monolayer of small adsorbate molecules, excitonic effects may be important. In this case, adding the optical gap of the neutral adsorbate, as observed in ELS, to the $HOMO^+$ BE gives only a poor lower limit on the position of $LUMO^-$ relative to E_F. An estimated $LUMO^-$ position can be obtained from the measured [51] electron affinity of gas-phase aniline, −1.13 eV, where the negative value means that the anion is unstable relative to the neutral molecule. Reducing this by ~0.5 eV to account for polarization in the adsorbed phase [49,50] places $LUMO^-$ roughly 0.5 eV above the vacuum level in Fig. 8. This of course neglects any chemical effect of adsorption on $LUMO^-$, which is difficult to model at the present level of theory (see below).

3.6. Quantum-chemical modeling of adsorbed aniline

Density functional theory (DFT) calculations, using the Gaussian 98 package [52], were done in order to relate the UPS data in Fig. 5a to candidate structural models for chemisorbed aniline. As a test, free molecular aniline was considered first. Geometry optimization, followed by a calculation of orbital energies, was done at the B3LYP/6-31G* level previously shown [53,54] to give reliable

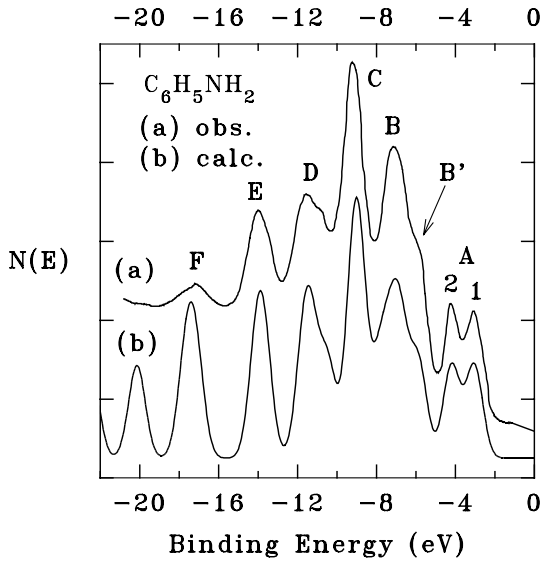

Fig. 9. (a) UPS data for condensed aniline (same as Fig. 5b), with binding energy referenced to the Fermi level. (b) Model UPS for molecular aniline obtained (see text) by convoluting the computed density of states with a Gaussian broadening function (FWHM = 1 eV) and aligning the two spectra at the HOMO. The relative $N(E)$ scales are arbitrary.

structural results for aniline. The final bond lengths and angles were in complete agreement with previous results [53].

Fig. 9 shows UPS data for a condensed multilayer (repeated from Fig. 5b) compared with the calculated density of states (DOS). The latter was obtained by centering a unit-area Gaussian (FWHM = 1.0 eV) at each eigenvalue, summing the total intensity and aligning the two spectra at the HOMO (A1). The relative intensities and peak separations are in fairly good agreement with the data, and the fine structure in peaks B and D is reproduced in the calculation. Also, the trend in C 1s BE for inequivalent sites around the phenyl ring follows the experimental result [39].

The DOS shows a state at −20.0 eV and another (partially off-scale) at −22.5 eV which lie below the range of the data. The corresponding eigenvectors show the former to consist of approximately equal contributions from the 2s/3s orbitals of all carbons not bonded to the $–NH_2$ and the latter to be comprised of the 2s/3s orbitals of the N and the adjacent C. The assignment of other peaks to

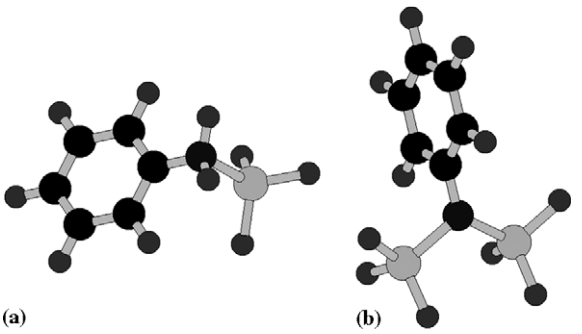

Fig. 10. Schematic diagrams (not to scale) of organometallic molecular models used in the quantum-chemical analysis of aniline adsorption on GaN(0 0 0 1). (a) Bonding to one GaH_3 and (b) bonding to two GaH_3 groups (see text). The large, lightly shaded spheres are Ga atoms.

specific molecular orbitals is discussed in [31]. The DOS takes no account of the dependence of photoionization cross-section, σ, on atomic orbital composition. Since $\sigma_{2p}/\sigma_{2s} = 1.6$ (4.0) for C (N) at $h\nu = 40.8$ eV [55], the DOS overestimates the UPS relative intensity of these deep-lying s-like molecular orbitals.

Fig. 10 shows schematic models of organometallic molecules designed to mimic various modes of bonding of aniline (abbreviated here as Φ–NH_2) to the GaN(0 0 0 1) surface. In Fig. 10a a donor–acceptor bond is formed involving the nitrogen NBLP orbital and the empty Ga orbital of GaH_3. In Fig. 10b, two H atoms are removed from $-NH_2$ leaving an sp^2-hybridized N with two NBLP orbitals each bonding to a GaH_3. Two variations (not shown) were also considered. In one, an H^+ is removed from the structure in Fig. 10a, resulting in a Φ–NH^- anion with one NBLP orbital. This is analogous to the NH_2–Ga species recently proposed [56] for the adsorption of NH_3 on Ga-deficient GaN(0 0 0 1) surfaces under growth conditions. In the other, an H^- is added to the structure in Fig. 10b, giving a Φ–$NH^-\lessgtr$ anion.

The use of anions in some of the adsorption models requires further comment. In bulk GaN, Ga has three valence electrons and bonds to four N's, and N has five valence electrons and bonds to four Ga's. Hence, each two-electron Ga–N bond involves an electron density equivalent to 0.75 |e| from Ga and 1.25 |e| from N. When a bond is broken to form a hypothetical ideal (0 0 0 1) surface Ga site, the dangling Ga orbital is occupied by 0.75 |e| before any charge or lattice relaxation. This fractional occupancy makes it difficult to construct a simple yet realistic cluster model for the ideally terminated surface. In invoking anions as adsorbate models, it is assumed that charge relaxation can occur on the real surface which results in an adsorbate electronic structure resembling that of a closed-shell anion. A detailed description of how this charge relaxation occurs would require a realistic surface model, since the simple electron counting given above suggests that sites in addition to those directly bonded to aniline would be involved. Here we are concerned only with characterizing the UPS spectra of the adsorbate species formed as the endpoint of this process.

For the various models discussed above, geometry optimization was done at the RHF/6-31G* level with no constraints imposed, beginning with a structure optimized using molecular mechanics, and orbital energies were computed at the B3LYP/6-31G* level. For comparison, B3LYP/6-31G* geometry optimizations were also done, starting from the RHF-optimized structure, with no difference in the final DOS results. The basis sets internal to the Gaussian 98 program package [52] were used for H, C and N. For Ga, the 6-31G* basis set recently given by Rassolov et al. [57] was used.

Fig. 11 shows the DOS calculated, as in Fig. 9b, for three of the four models outlined above. The fourth, with neutral Φ–$N\lessgtr$ bridging two GaH_3 groups (as in Fig. 10b), was found to be unstable. The RHF geometry optimization in this case resulted in the breaking of both Ga–N bonds and a shorter C–N bond (1.29 Å) than in free Φ–NH_2 (1.40 Å), suggesting a degree of N π-bonding in the former. For direct comparison with $\Delta N(E)$, each calculated DOS includes only the contributions from the adsorbate Φ–NH_2 or Φ–NH^- species. All spectra have been aligned at the deepest experimentally observed level, at about −18 eV, corresponding to peak "F" in Fig. 9a, and the calculated spectra have been Gaussian-broadened by 1.0 eV as in Fig. 9b. As noted above, the relative intensities of the deep s-like states are overestimated in the calculated DOS, and the nearly

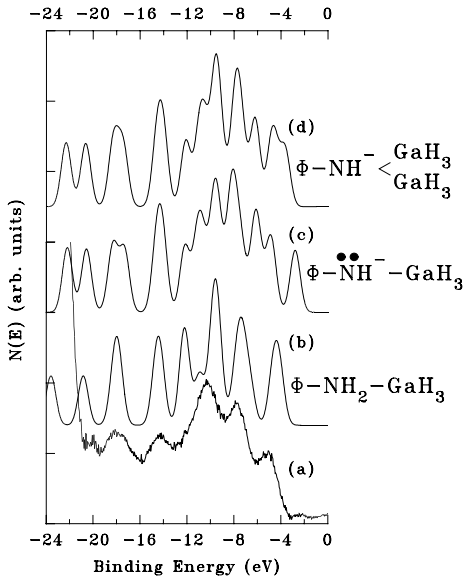

Fig. 11. Experimental (a) and DFT (b)–(d) results for the HeII UPS of adsorbed aniline, Φ–NH_2 (see text). (a) Experimental [same as Fig. 5a]; (b) Φ–NH_2–GaH_3 [aniline forming donor–acceptor adduct with GaH_3 via the –NH_2 non-bonding lone-pair orbital]; (c) Φ–$(NH)^-$–GaH_3 [an H^+ is removed from (b) to form an anion with an N non-bonding lone-pair orbital (••)]; (d) Φ–$(NH)^-$–$(GaH_3)_2$ [like (c) but a second GaH_3 bonds via N lone pair]. The DFT results have all been Gaussian-broadened with a 1.0 eV FWHM for comparison with Figs. 9a and b, and all spectra have been aligned at the deep-valence peak at about −18 eV (peak "F" in Fig. 9). For direct comparison with the $\Delta N(E)$ data, each calculated DOS includes only the contributions from the adsorbate Φ–NH_2 or Φ–NH^- species.

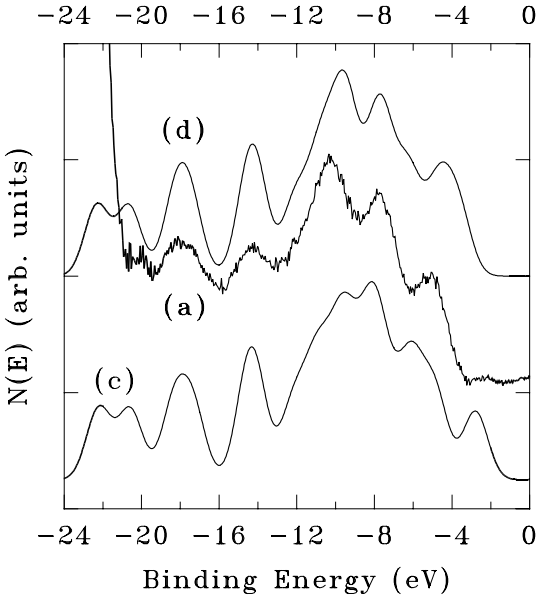

Fig. 12. Similar to Fig. 11 but with an increased Gaussian broadening of the calculated spectra (1.5 eV FWHM) to match approximately that of the $\Delta N(E)$ data. The labels (a), (c) and (d) correspond to those in Fig. 11.

pure s-states below −20 eV cannot be seen clearly in the present experimental spectrum.

The simplest model, in which Φ–NH_2 forms a donor–acceptor pair with a single GaH_3, clearly does not fit the data as shown in Fig. 11b. Here a peak is seen at −12 eV, corresponding to peak "D" in Fig. 9, which is due to an orbital with a large –NH_2 contribution and which is absent in the experimental spectrum. Of the remaining two models, that in Fig. 11d appears to be in better agreement, particularly in the position of the HOMO. For direct comparison with experiment, Fig. 12 shows the calculated results in Figs. 11c and d with a larger Gaussian broadening (1.5 vs 1.0 eV) to better approximate that of the HeII UPS. As noted above, the instrumental resolution is 0.8 eV which, when subtracted in quadrature from the ∼1.5 eV total broadening, leaves ∼1.3 eV from "solid-state effects". Better agreement is clearly seen for Fig. 12d, corresponding to a Φ–$NH^-<$ group forming a Ga–N–Ga bridge. This is analogous to the $NH_2<$ bridge previously proposed [7] for the adsorption of NH_3 on this surface.

4. Summary

Adsorption of aniline on the GaN(0 0 0 1)-(1×1) surface has been studied using mainly XAES, ELS and UPS. The results are as follows.

1. The XAES data show adsorption near room temperature with a total sticking probability of ∼0.05 and a saturation coverage of ∼0.28 phenyl rings per surface lattice site. In contrast, benzene does not chemisorb readily under these conditions.
2. The ELS data show removal of the characteristic surface-state band, centered at ∼3.4 eV, and the appearance of a $\pi \rightarrow \pi^*$ loss at 6.5 eV due to C=C bonds.

3. The UPS data, which have been analyzed with the aid of DFT calculations, indicate adsorption with the phenyl ring and the phenyl–N bond remaining intact. Bonding occurs in the form of a phenyl–NH group via a Ga–N–Ga bridge, analogous to the model previously proposed [7] for the adsorption of NH_3 on this surface.
4. Adsorption causes a decrease in electron affinity ($\delta\chi \approx -0.55$ eV) due to a surface dipole layer, and measurement of $\delta\chi$ and of changes in band bending have been used to construct a partial energy level diagram for the aniline-covered surface. The adsorbate $HOMO^+$ lies well below the VBM, while the $LUMO^-$ is estimated to lie roughly 0.5 eV above the vacuum level.

The present results demonstrate that organic amines can easily be used for the attachment of functional groups to the GaN(0 0 0 1) surface, and the energy level alignment deduced from the data provides a rational basis for designing chemical processes involving hot-electron transport across the semiconductor/organic interface. Further experimental work on amine/GaN systems would be very useful. In particular, a vibrational probe such as high-resolution electron energy loss spectroscopy (HREELS) could in principle help in refining the chemisorption model. However, previous HREELS studies of adsorption on wurtzite GaN surfaces [20,25,65] show that strong features due to multiple excitations of the surface longitudinal optic (Fuchs–Kliewer) mode make it difficult to identify adsorbate losses below $\sim$2000 cm^{-1} ($\sim$250 meV), where modes other than the C–H and N–H stretches are expected.

Acknowledgements

This work was supported by the Office of Naval Research and also in part by a grant of computer time from the DOD High-Performance Computing Modernization Program at the ASC-MSRC, Wright-Patterson AFB. A.E. Wickenden and D.D. Koleske are gratefully acknowledged for providing the GaN sample. A.E. Berry is thanked for help in purifying the aniline. A critical reading of the manuscript by J.P. Long is gratefully acknowledged, and A. Kahn, V.J. Bellitto and J.N. Russell Jr. are thanked for numerous helpful discussions.

Appendix A

This appendix describes the use of the C KLL and N KLL XAES data to obtain the coverage of phenyl rings, Θ_{ph}. The procedure is similar to that used in previous studies [17,58] of adsorption on GaN. First, a linear background, fitted to the region above the spectrum, is subtracted and the result corrected for the $1/E$ dependence of the CMA "étendue" (product of transmission and area sampled) in constant-resolution mode [59]. Since the data were obtained in counting, rather than analog, mode no correction for an energy-dependent detector gain is needed. The spectrum is then processed following Tougaard [60,61] to remove the inelastic background and the final result (Fig. 3) integrated to give I_C or I_N.

Fig. 13 shows a schematic diagram of the model used to estimate Θ_{ph}. The ratio of C KLL and N KLL integrated areas (I_C/I_N) is given by

$$\frac{I_C}{I_N} = 6\Theta_{ph}S_C \Big/ \left(S_N \exp(-d_C/\lambda_C \cos\phi) \times \left[\Theta_{ph} + \exp(-\delta/\lambda_{GaN}\cos\phi) \times \sum_{n=0}^{\infty} \exp(-nd_{GaN}/\lambda_{GaN}\cos\phi) \right] \right).$$

In the denominator, the sum accounts for the substrate signal and the term in δ for the attenuation by the terminating Ga layer. The Θ_{ph} term is the contribution from adsorbed N in the aniline layer, and the term in d_C gives the attenuation of the entire N KLL intensity by the phenyl overlayer, assumed to be continuous at saturation. The numerator gives the C KLL intensity with the assumption that all six phenyl carbons contribute equally.

The thickness values $d_{GaN} = 2.59$ Å, $\delta = 0.648$ Å and $d_C = 1.4$ Å are defined in Fig. 13. The first two come from the wurtzite GaN lattice parameters and the last from the dimensions of a phenyl ring tipped 30° away from the surface normal. The

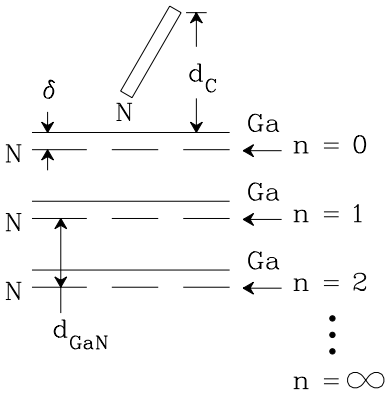

Fig. 13. Schematic model (not to scale) of aniline adsorbed on GaN(0 0 0 1)-(1 × 1) used to compute the C KLL/N KLL XAES relative intensity. The numbering of the N-planes is indicated, and the rectangle represents a side view of the phenyl ring.

terms λ_{GaN} and λ_C are the effective attenuation lengths for N KLL electrons (~370 eV) in GaN and in the phenyl layer (modeled as pure carbon), respectively. Values of $\lambda_{GaN} = 7.20$ Å and $\lambda_C = 11.6$ Å were obtained using a standard database [4] which includes the effects of elastic scattering [62]. The CMA collection angle is $\phi = 42°$. S_C, the C KLL XAES sensitivity factor, is the product of the Mg Kα K-shell photoionization cross-section [σ(C 1s)] and the Auger decay probability [ρ(C KLL)]. S_N is defined analogously. Values of $\sigma(\text{C 1s}) = 0.022$ and $\sigma(\text{N 1s}) = 0.039$ (in units of 10^6 barns) are given by Yeh and Lindau [55]. The estimated values [63,64] for ρ(C KLL) and ρ(N KLL) are virtually identical and cancel in the S_C/S_N ratio. Of the quantities used here, the most uncertain is d_C. However, varying d_C by a factor of 2 changes Θ_{ph} by only ~12%, which is comparable to the effect of scatter in the data.

References

[1] R.J. Hamers, S.K. Coulter, M.D. Ellison, J.S. Hovis, D.F. Padowitz, M.P. Schwartz, C.M. Greenlief, J.N. Russell Jr., Acc. Chem. Res. 33 (2000) 617.
[2] J.M. Buriak, Chem. Commun. (1999) 1051.
[3] R.A. Wolkow, Annu. Rev. Phys. Chem. 50 (1999) 413.
[4] F. Seker, K. Meeker, T.F. Kuech, A.B. Ellis, Chem. Rev. 100 (2000) 2505.
[5] K. Gartsman, D. Cahen, A. Kadyshevitch, J. Libman, T. Moav, R. Naaman, A. Shanzer, V. Umansky, A. Vilan, Chem. Phys. Lett. 283 (1998) 301.
[6] R. Cohen, L. Kronik, A. Shanzer, D. Cahen, A. Liu, Y. Rosenwaks, J.K. Lorenz, A.B. Ellis, J. Am. Chem. Soc. 121 (1999) 10545.
[7] V.M. Bermudez, Chem. Phys. Lett. 317 (2000) 290.
[8] X. Chen, K.E. Gonsalves, M.-I. Baraton, Chem. Mater. 9 (1997) 328.
[9] M.-I. Baraton, G. Carlson, K.E. Gonsalves, Mater. Sci. Eng. B 50 (1997) 42.
[10] Th. Kugler, Ch. Ziegler, W. Göpel, Mater. Sci. Eng. B 37 (1996) 112.
[11] T. Bitzer, T. Alkunshalie, N.V. Richardson, Surf. Sci. 368 (1996) 202.
[12] R.-M. Rummel, C. Ziegler, Surf. Sci. 418 (1998) 303.
[13] X.-Y. Zhu, J.A. Mulder, W.F. Bergerson, Langmuir 15 (1999) 8147.
[14] X. Cao, S.K. Coulter, M.D. Ellison, H. Liu, J. Liu, R.J. Hamers, J. Phys. Chem. B 105 (2001) 3759.
[15] H. Tomimoto, R. Sumii, N. Shirota, S. Yagi, M. Taniguchi, T. Sekitani, K. Tanaka, J. Vac. Sci. Technol. B 18 (2000) 2335.
[16] V.M. Bermudez, J.P. Long, Surf. Sci. 450 (2000) 98.
[17] V.M. Bermudez, J. Appl. Phys. 80 (1996) 1190.
[18] V.M. Bermudez, D.D. Koleske, A.E. Wickenden, Appl. Surf. Sci. 126 (1998) 69.
[19] O. Janzen, Ch. Hahn, T.U. Kampen, W. Mönch, Eur. Phys. J. B 7 (1999) 1.
[20] S. Sloboshanin, F.S. Tautz, V.M. Polyakov, U. Starke, A.S. Usikov, B.Ja. Ber, J.A. Schaefer, Surf. Sci. 427–428 (1999) 250.
[21] E.S. Hellman, MRS Internet J. Nitride Semicond. Res. 3 (1998) 11.
[22] C.J. Powell, Appl. Surf. Sci. 89 (1995) 141.
[23] C.T. Campbell, S.M. Valone, J. Vac. Sci. Technol. A 3 (1985) 408.
[24] V.J. Bellitto, B.D. Thoms, D.D. Koleske, A.E. Wickenden, R.L. Henry, Phys. Rev. B 60 (1999) 4816.
[25] S.P. Grabowski, H. Nienhaus, W. Mönch, Surf. Sci. 454–456 (2000) 498.
[26] T. Ari, H. Güven, N. Ecevit, J. Electron Spectrosc. Relat. Phenom. 73 (1995) 13.
[27] H.-P. Steinruck, J. Phys. Condens. Matter 8 (1996) 6465.
[28] C.I. Wu, A. Kahn, J. Appl. Phys. 86 (1999) 3209.
[29] Y.-C. Chao, C.B. Stagarescu, J.E. Downes, P. Ryan, K.E. Smith, D. Hanser, M.D. Bremser, R.F. Davis, Phys. Rev. B 59 (1999) 15586.
[30] M.G. Ramsey, G. Rosina, D. Steinmüller, H.H. Graen, F.P. Netzer, Surf. Sci. 232 (1990) 266.
[31] M.H. Palmer, W. Moyes, M. Spiers, J.N.A. Ridyard, J. Mol. Struct. 53 (1979) 235.

[4] See http://www.nist.gov/srd/nist82.htm for information on obtaining this database.

[32] S. Gokhale, P. Trischberger, D. Menzel, W. Widdra, H. Dröge, H.-P. Steinrück, U. Birkenheuer, U. Gutdeutsch, N. Rösch, J. Chem. Phys. 108 (1998) 5554.
[33] J.E. Demuth, D.E. Eastman, Phys. Rev. Lett. 32 (1974) 1123.
[34] H. Ågren, P.S. Bagus, J. Am. Chem. Soc. 107 (1985) 134.
[35] P. Barta, Th. Kugler, W.R. Salaneck, A.P. Monkman, J. Libert, R. Lazzaroni, J.L. Brédas, Synth. Met. 93 (1998) 83.
[36] S.X. Huang, D.A. Fischer, J.L. Gland, J. Phys. Chem. 100 (1996) 10223.
[37] V.M. Bermudez, J.P. Long, Appl. Phys. Lett. 66 (1995) 475.
[38] J.L. Solomon, R.J. Madix, J. Stöhr, Surf. Sci. 255 (1991) 12.
[39] T. Ohta, T. Fujikawa, H. Kuroda, Bull. Chem. Soc. Jpn. 48 (1975) 2017.
[40] W. Mönch, Semiconductor Surfaces and Interfaces, Springer, Berlin, 1993 (Chapter 14).
[41] J. Waite, M.G. Papadopoulos, J. Chem. Phys. 82 (1985) 1427.
[42] D.G. Lister, J.K. Tyler, J.H. Høg, N. Wessel Larsen, J. Mol. Struct. 23 (1974) 253.
[43] C. Bandis, B.B. Pate, Surf. Sci. 345 (1996) L23.
[44] K. Besocke, S. Berger, Rev. Sci. Instrum. 47 (1976) 840.
[45] J.L. Gland, G.A. Somorjai, Surf. Sci. 41 (1974) 387.
[46] A. Many, Y. Goldstein, N.B. Grover, Semiconductor Surfaces, North-Holland, Amsterdam, 1965 (Chapter 2).
[47] B.K. Meyer, D. Volm, A. Graber, H.C. Alt, T. Detchprohm, A. Amano, I. Akasaki, Solid State Commun. 95 (1995) 597.
[48] J.R. Waldrop, R.W. Grant, Appl. Phys. Lett. 68 (1996) 2879.
[49] C.I. Wu, Y. Hirose, H. Sirringhaus, A. Kahn, Chem. Phys. Lett. 272 (1997) 43.
[50] I.G. Hill, A. Kahn, Z.G. Soos, R.A. Pascal Jr., Chem. Phys. Lett. 327 (2000) 181.
[51] K.D. Jordan, J.A. Michejda, P.D. Burrow, J. Am. Chem. Soc. 98 (1976) 7189.
[52] M.J. Frisch et al., Gaussian 98 (Revision A.9), Gaussian, Inc., Pittsburgh, PA, 1998.
[53] M.E. Vaschetto, B.A. Retamal, A.P. Monkman, J. Mol. Struct. Theochem 468 (1999) 209.
[54] M.A. Mora, L. Galicia, H. Vázquez, Int. J. Quantum Chem. 78 (2000) 99.
[55] J.J. Yeh, I. Lindau, Atom. Data Nucl. Data Tables 32 (1985) 1.
[56] C.A. Pignedoli, R. Di Felice, C.M. Bertoni, Phys. Rev. B 64 (2001) (Art. no. 113301).
[57] V.A. Rassolov, M.A. Ratner, J.A. Pople, P.C. Redfern, L.A. Curtis, J. Comput. Chem. 22 (2001) 976.
[58] V.M. Bermudez, Appl. Surf. Sci. 119 (1997) 147.
[59] M.P. Seah, in: D. Briggs, M.P. Seah (Eds.), Practical Surface Analysis, first ed., Wiley, Chichester, 1983 (Chapter 5).
[60] S. Tougaard, Surf. Interface Anal. 11 (1988) 453.
[61] S. Tougaard, Surf. Sci. 216 (1989) 343.
[62] C.J. Powell, A. Jablonski, NIST Electron Effective-Attenuation-Length Database (NIST Standard Reference Database 82), US National Institute of Standards and Technology, Gaithersburg, MD, 2001.
[63] S. Mroczkowski, D. Lichtman, J. Vac. Sci. Technol. A 3 (1985) 1860.
[64] S. Mroczkowski, J. Vac. Sci. Technol. A 7 (1989) 1529.
[65] V.J. Bellitto, B.D. Thoms, D.D. Koleske, A.E. Wickenden, R.L. Henry, Surf. Sci. 430 (1999) 80.